

RG-Consistent (P)NJL Model: Impact of Thermal Cutoff Modifications on Thermodynamics and Net-Baryon Number Fluctuations

Jie Tang, Fan Lin,* and Xinyang Wang†

*Center for Fundamental Physics, School of Mechanics and Physics,
Anhui University of Science and Technology, Huainan, Anhui 232001, People's Republic of China*

(Dated: May 12, 2026)

In this paper, we investigate the impact of renormalization group (RG) consistency on the chiral phase transition and thermodynamic properties of QCD matter using the RGNJL and RGNJL models. By implementing a temperature-dependent thermal cutoff $\Lambda_T = k\Lambda_0$, we ensure that thermodynamic quantities converge toward the Stefan-Boltzmann limit at high temperatures, effectively extending the applicability of these effective theories. Our analysis shows that while the RG-consistency condition ($k \rightarrow \infty$) resolves causality violations in the RGNJL model by binding the speed of sound to the conformal limit, the RGNJL model exhibits a more complex, non-monotonic sensitivity to the parameter k . Furthermore, we demonstrate that the RG-improved PNJL framework significantly enhances the description of net-baryon number fluctuations ($\kappa\sigma^2$) relative to lattice QCD data at vanishing chemical potential, though the intensification of these fluctuations at high baryon density highlights a critical sensitivity to the model's parametric constraints. This study provides a rigorous evaluation of the RG-consistency framework's predictive power in mapping the QCD phase diagram and interpreting experimental observables.

I. INTRODUCTION

The properties of Quantum Chromodynamics (QCD) matter at finite temperature and baryon density constitute one of the central frontiers in high-energy physics. Theoretical studies predict that QCD matter undergoes phase transitions as the temperature and baryon density increase [1–3]. Current theoretical understanding suggests that the chiral phase transition of QCD proceeds as a smooth crossover at low baryon chemical potential (μ_B), while it is expected to turn into a first-order phase transition at larger μ_B . The endpoint separating these two regimes is commonly referred to as the QCD critical point [4, 5]. Near this critical point, long-range correlations develop and the correlation length of the system grows significantly [6]. As a consequence, event-by-event fluctuations of conserved charges become strongly enhanced [7]. In particular, the cumulants of the net-proton number, which are sensitive to the correlation length, are expected to exhibit characteristic critical behavior and may even diverge in the vicinity of the critical point. Over the past decade, extensive experimental efforts have therefore been devoted to searching for signatures of the QCD critical point through measurements of fluctuation observables [8, 9]. These fluctuation observables, or equivalently the corresponding susceptibilities, provide an important experimental probe for mapping the structure of the QCD phase diagram. Recent experimental results [10, 11] report significant signals in the ratio C_4/C_2 , which may serve as a characteristic indicator of nontrivial structures in the QCD phase diagram.

In the theoretical regime, the infrared behavior of QCD is difficult to address due to its intrinsically non-perturbative nature. Lattice QCD provides a powerful first-principles approach; however, it still suffers from the well-known sign problem at finite baryon density. Consequently, effective field theories remain one of the most practical and reliable approaches for exploring non-perturbative aspects of QCD. Among these approaches, the Nambu–Jona-Lasinio (NJL) model [12–15] is one of the most widely used low-energy effective theories of QCD, particularly for studying spontaneous chiral symmetry breaking and its restoration at finite temperature and density [16–18]. To incorporate aspects of gluon dynamics, the Polyakov loop is introduced, leading to the so-called Polyakov–Nambu–Jona-Lasinio (PNJL) model [19]. This extension enables a simultaneous investigation of the chiral phase transition and the confinement/deconfinement transition within an effective field theory framework [1, 20, 21]. Nevertheless, as four-fermion interaction theories, both the NJL and PNJL models are non-renormalizable. As a consequence, the choice of regularization scheme becomes an essential component of the model and remains under active discussion. In practice, various cutoff schemes are employed to regularize the vacuum contribution, including hard or smooth cutoffs in three-momentum or four-momentum space [14, 15]. For the thermal contribution, however, it is still debated whether regularization is necessary; a detailed discussion can be found in Ref. [22–25].

Recently, renormalization group (RG) consistency has been implemented in low-energy effective theories (LEFTs) to extend their applicability in hot and dense systems [26, 27]. In general, a LEFT in vacuum is defined with a finite

* linfan@aust.edu.cn (Corresponding Author)

† wangxy@aust.edu.cn

ultraviolet cutoff Λ_0 ; for the NJL model, one typically has $\Lambda_0 \simeq 600$ MeV. However, in a medium with temperature or chemical potential exceeding Λ_0 , contributions from higher momentum scales can become relevant, thereby challenging the validity of a fixed cutoff treatment. To maintain RG consistency, the full quantum effective action Γ is required to be independent of the cutoff scale,

$$\lim_{\Lambda \rightarrow +\infty} \Lambda \frac{d\Gamma}{d\Lambda} = 0, \quad (1)$$

which imposes nontrivial constraints on the ultraviolet regulator and ensures that physical observables remain insensitive to its specific choice. This framework has recently been applied to the NJL model (RG-improved NJL, or RGNJL) in Ref. [28, 29] to investigate color superconductivity. Although the RG procedure extends the applicability of the non-renormalizable NJL model to hot and dense regimes, it remains unclear whether the RGNJL framework resolves the inconsistencies associated with cutoff artifacts identified in previous studies [23]. Furthermore, it is important to systematically examine how the RG implementation modifies the predictions of the NJL/PNJL models and to assess their consistency with the latest experimental observations.

In this study, we present a systematic analysis of the RG-improved NJL (RGNJL) model, focusing on the impact of RG implementation on the chiral phase transition, thermodynamic properties, and baryon number susceptibilities. To facilitate a more direct comparison with experimental data and to incorporate confinement-related effects, we further extend the analysis to the RG-consistent Polyakov-loop-extended Nambu–Jona–Lasinio (RGPNJL) model. By confronting our results with recent experimental measurements, we assess the reliability and predictive power of the RG-consistency framework.

The paper is organized as follows. In Sec. II, we review the theoretical framework of the RG(P)NJL model and discuss the associated regularization schemes. In Sec. III, we analyze the chiral phase transition within this framework. In Sec. IV, we present results for thermodynamic quantities and baryon number fluctuations. Finally, Sec. V contains a summary and an outlook for future research.

II. FORMALISM

In this section, we introduce the two-flavor RG-improved NJL/PNJL models, which are among the most widely used low-energy effective theories of QCD.

The Lagrangian density of the two-flavor NJL model is given by

$$\mathcal{L}_{\text{NJL}} = \bar{\psi} (i\gamma^\mu \partial_\mu - \hat{m}) \psi + G_S \left[(\bar{\psi}\psi)^2 + (\bar{\psi}i\gamma^5 \boldsymbol{\tau}\psi)^2 \right], \quad (2)$$

where $\psi = (u, d)^T$ denotes the two-flavor quark field, and $\hat{m} = \text{diag}(m_u, m_d)$ is the current quark mass matrix. For simplicity, we assume isospin symmetry, $m_u = m_d = m$. The Pauli matrices $\boldsymbol{\tau} = (\tau^1, \tau^2, \tau^3)$ act in flavor space. The coupling constant G_S characterizes the interaction strength in the scalar and pseudoscalar channels.

Within the mean-field approximation, quantum fluctuations around the condensates are neglected, and the four-fermion interactions can be linearized as

$$(\bar{\psi}\psi)^2 = 2\langle\bar{\psi}\psi\rangle\bar{\psi}\psi - \langle\bar{\psi}\psi\rangle^2, \quad (\bar{\psi}i\gamma^5 \boldsymbol{\tau}\psi)^2 = 2\langle\bar{\psi}i\gamma^5 \boldsymbol{\tau}\psi\rangle\bar{\psi}i\gamma^5 \boldsymbol{\tau}\psi - \langle\bar{\psi}i\gamma^5 \boldsymbol{\tau}\psi\rangle^2. \quad (3)$$

Here, $\langle\bar{\psi}\psi\rangle$ and $\langle\bar{\psi}i\gamma^5 \boldsymbol{\tau}\psi\rangle$ denote the chiral and pseudoscalar condensates, respectively. In the absence of an axial chemical potential μ_5 , the pseudoscalar condensate vanishes, $\langle\bar{\psi}i\gamma^5 \boldsymbol{\tau}\psi\rangle = 0$. The Lagrangian density then reduces to

$$\mathcal{L}_{\text{NJL}} = \bar{\psi} (i\gamma^\mu \partial_\mu - \hat{m} + 2G_S\langle\bar{\psi}\psi\rangle) \psi - G_S\langle\bar{\psi}\psi\rangle^2 = \bar{\psi} (i\gamma^\mu \partial_\mu - M) \psi - \frac{(M - m)^2}{4G_S}, \quad (4)$$

where we have introduced the constituent quark mass $M = m - 2G_S\langle\bar{\psi}\psi\rangle$.

The constituent quark mass is determined self-consistently from the thermodynamic potential once finite temperature and chemical potential effects are taken into account. Following standard procedures [14, 15, 30], the grand thermodynamic potential at the one-loop level for finite temperature T and chemical potential of quark μ can be written as

$$\Omega_{\text{NJL}} = \frac{(M - m)^2}{4G_S} - 2N_c N_f \int \frac{d^3p}{(2\pi)^3} \left[E + T \ln \left(1 + e^{-\beta(E - \mu)} \right) + T \ln \left(1 + e^{-\beta(E + \mu)} \right) \right], \quad (5)$$

where $\beta = 1/T$ and $E = \sqrt{p^2 + M^2}$ denotes the single-particle dispersion relation of the constituent quark. The physical value of the constituent quark mass is obtained by minimizing the thermodynamic potential, which is equivalent

to solving the gap equation

$$\frac{d\Omega_{\text{NJL}}}{dM} = 0, \quad (6)$$

However, this equation cannot be solved without further specification, since the NJL model is non-renormalizable and the momentum integral is ultraviolet divergent. Therefore, an appropriate regularization scheme must be introduced before proceeding with the numerical evaluation.

In practice, the ultraviolet divergence in the vacuum contribution is typically treated by introducing a momentum cutoff. A common choice is the three-momentum regularization scheme. For instance, in the hard-cutoff scheme, the upper limit of the momentum integral is replaced by a finite cutoff Λ , i.e., the integration range is restricted from $[0, \infty)$ to $[0, \Lambda]$. In contrast, for the thermal contribution to the thermodynamic potential, it remains under debate whether a similar cutoff should be imposed. As discussed in Ref. [23], applying the cutoff to the finite (thermal) part of the integral may lead to inconsistencies, and different prescriptions can yield qualitatively different results. Recently, the implementation of RG consistency in effective theories has provided a more systematic framework to address this issue and further clarify the role of the cutoff in both vacuum and thermal contributions.

As shown in Ref. [28], imposing the RG consistency condition in Eq. (1) on the NJL model modifies the regularization procedure. In particular, an additional cutoff scale is introduced for the thermal contribution, which can be parameterized as $\Lambda_T = k \Lambda_0$. In general, for a medium with temperature or chemical potential exceeding the vacuum cutoff scale Λ_0 , contributions from higher momentum modes become relevant. This implies that the parameter k should satisfy $k \geq 1$, with its precise value determined by the physical conditions under consideration. Accordingly, the grand thermodynamic potential of the RG-improved NJL (RGNJL) model can be expressed as

$$\Omega_{\text{RGNJL}} = \frac{(M - m)^2}{4G_S} - 2N_c N_f \int_0^{\Lambda_0} \frac{d^3p}{(2\pi)^3} E - 2N_c N_f T \int_0^{\Lambda_T} \frac{d^3p}{(2\pi)^3} \left[\ln \left(1 + e^{-\beta(E-\mu)} \right) + \ln \left(1 + e^{-\beta(E+\mu)} \right) \right], \quad (7)$$

where $\Lambda_T = k \Lambda_0$ explicitly separates the cutoff scales for the vacuum and thermal contributions.

While the NJL model successfully describes the chiral phase transition, it lacks confinement dynamics. This limitation motivates the extension to the RG-consistent two-flavor PNJL model. The order parameter for the confinement/deconfinement phase transition is the Polyakov loop,

$$L(\vec{x}) = \mathcal{P} \exp \left[i \int_0^{1/T} d\tau A_4(\vec{x}, \tau) \right], \quad (8)$$

where A_4 denotes the temporal component of the background gluon field. The traced Polyakov loop and its conjugate are defined as

$$\Phi = \frac{\text{Tr}_c L}{N_c}, \quad \bar{\Phi} = \frac{\text{Tr}_c L^\dagger}{N_c}, \quad (9)$$

which effectively act as imaginary chemical potentials for quarks and can be incorporated into the thermodynamic potential [19, 31–33].

The grand thermodynamic potential of the RGPNJL model then takes the form

$$\begin{aligned} \Omega_{\text{RGPNJL}} &= \frac{(M - m)^2}{4G_S} + \mathcal{U}(\Phi, \bar{\Phi}, T) - 2N_c N_f \int_0^{\Lambda_0} \frac{d^3p}{(2\pi)^3} E \\ &\quad - 2N_f T \int_0^{\Lambda_T} \frac{d^3p}{(2\pi)^3} \ln \left(1 + 3\Phi e^{-\beta(E-\mu)} + 3\bar{\Phi} e^{-2\beta(E-\mu)} + e^{-3\beta(E-\mu)} \right) \\ &\quad - 2N_f T \int_0^{\Lambda_T} \frac{d^3p}{(2\pi)^3} \ln \left(1 + 3\bar{\Phi} e^{-\beta(E+\mu)} + 3\Phi e^{-2\beta(E+\mu)} + e^{-3\beta(E+\mu)} \right), \end{aligned} \quad (10)$$

where the same separation of cutoff scales has been applied to the thermal contributions. The effective potential $\mathcal{U}(\Phi, \bar{\Phi}, T)$ encodes the gluonic degrees of freedom and cannot be derived directly from QCD. A commonly used phenomenological parametrization is [31, 34, 35]

$$\frac{\mathcal{U}(\Phi, \bar{\Phi}, T)}{T^4} = -\frac{a(T)}{2} \bar{\Phi} \Phi + b(T) \ln \left[1 - 6\bar{\Phi} \Phi + 4(\bar{\Phi}^3 + \Phi^3) - 3(\bar{\Phi} \Phi)^2 \right], \quad (11)$$

where $a(T) = a_0 + a_1 \left(\frac{T_0}{T}\right) + a_2 \left(\frac{T_0}{T}\right)^2$ and $b(T) = b_3 \left(\frac{T_0}{T}\right)^3$.

Before solving the RGNJL/RGPNJL models and analyzing the corresponding physical effects, the model parameters must be fixed to reproduce basic hadronic observables in vacuum, such as the pion mass $m_\pi = 139.3 \text{ MeV}$ and the pion decay constant $f_\pi = 92 \text{ MeV}$. In this work, we adopt the standard parameter set $m_u = m_d = 5.5 \text{ MeV}$, $N_c = 3$, $N_f = 2$ together with $\Lambda_0 = 651 \text{ MeV}$, $G_S = 5.04 \text{ GeV}^{-2}$ which are used consistently in both the RGNJL and RGPNJL models. For the RGPNJL model, the parameters in the Polyakov-loop effective potential are chosen as $a_0 = 3.51$, $a_1 = -2.47$, $a_2 = 15.22$, $b_3 = -1.75$ which are fixed phenomenologically to reproduce lattice QCD results in the pure gauge sector [31, 34, 35].

III. CHIRAL PHASE TRANSITION

The physical constituent quark mass is determined by minimizing the thermodynamic potential. By solving the corresponding gap equation, one obtains the constituent quark mass as a function of temperature and chemical potential for a given RG-modified thermal cutoff $\Lambda_T = k \Lambda_0$.

For the RGNJL model, the gap equation reads

$$\frac{\partial \Omega_{\text{RGNJL}}}{\partial M} = \frac{M - m}{2G_S} - 2N_c N_f \int_0^{\Lambda_0} \frac{d^3 p}{(2\pi)^3} \frac{M}{E} + 2N_c N_f \int_0^{\Lambda_T} \frac{d^3 p}{(2\pi)^3} \frac{M}{E} \left[\frac{1}{1 + e^{\beta(E-\mu)}} + \frac{1}{1 + e^{\beta(E+\mu)}} \right] = 0. \quad (12)$$

Similarly, for the RGPNJL model, the stationarity conditions with respect to M , Φ , and $\bar{\Phi}$ lead to a coupled set of gap equations. The gap equation for the constituent quark mass is given by

$$\begin{aligned} \frac{\partial \Omega_{\text{RGPNJL}}}{\partial M} &= \frac{M - m}{2G_S} - 2N_c N_f \int_0^{\Lambda_0} \frac{d^3 p}{(2\pi)^3} \frac{M}{E} \\ &+ 2N_f \int_0^{\Lambda_T} \frac{d^3 p}{(2\pi)^3} \frac{M}{E} \frac{3\Phi e^{-\beta(E-\mu)} + 6\bar{\Phi} e^{-2\beta(E-\mu)} + 3e^{-3\beta(E-\mu)}}{1 + 3\Phi e^{-\beta(E-\mu)} + 3\bar{\Phi} e^{-2\beta(E-\mu)} + e^{-3\beta(E-\mu)}} \\ &+ 2N_f \int_0^{\Lambda_T} \frac{d^3 p}{(2\pi)^3} \frac{M}{E} \frac{3\bar{\Phi} e^{-\beta(E+\mu)} + 6\Phi e^{-2\beta(E+\mu)} + 3e^{-3\beta(E+\mu)}}{1 + 3\bar{\Phi} e^{-\beta(E+\mu)} + 3\Phi e^{-2\beta(E+\mu)} + e^{-3\beta(E+\mu)}} = 0. \end{aligned} \quad (13)$$

The stationarity conditions with respect to the Polyakov loop variables Φ and $\bar{\Phi}$ are given by

$$\begin{aligned} \frac{\partial \Omega_{\text{RGPNJL}}}{\partial \bar{\Phi}} &= T^4 \left[-\frac{a(T)}{2} \bar{\Phi} + b(T) \frac{-6\bar{\Phi} + 12\Phi^2 - 6\bar{\Phi}^2\Phi}{1 - 6\bar{\Phi}\Phi + 4(\bar{\Phi}^3 + \Phi^3) - 3(\bar{\Phi}\Phi)^2} \right] \\ &- 2N_f T \int_0^{\Lambda_T} \frac{d^3 p}{(2\pi)^3} \frac{3e^{-\beta(E-\mu)}}{1 + 3\Phi e^{-\beta(E-\mu)} + 3\bar{\Phi} e^{-2\beta(E-\mu)} + e^{-3\beta(E-\mu)}} \\ &- 2N_f T \int_0^{\Lambda_T} \frac{d^3 p}{(2\pi)^3} \frac{3e^{-\beta(E+\mu)}}{1 + 3\bar{\Phi} e^{-\beta(E+\mu)} + 3\Phi e^{-2\beta(E+\mu)} + e^{-3\beta(E+\mu)}} = 0, \end{aligned} \quad (14)$$

$$\begin{aligned} \frac{\partial \Omega_{\text{RGPNJL}}}{\partial \Phi} &= T^4 \left[-\frac{a(T)}{2} \Phi + b(T) \frac{-6\Phi + 12\bar{\Phi}^2 - 6\bar{\Phi}\Phi^2}{1 - 6\bar{\Phi}\Phi + 4(\bar{\Phi}^3 + \Phi^3) - 3(\bar{\Phi}\Phi)^2} \right] \\ &- 2N_f T \int_0^{\Lambda_T} \frac{d^3 p}{(2\pi)^3} \frac{3e^{-2\beta(E-\mu)}}{1 + 3\Phi e^{-\beta(E-\mu)} + 3\bar{\Phi} e^{-2\beta(E-\mu)} + e^{-3\beta(E-\mu)}} \\ &- 2N_f T \int_0^{\Lambda_T} \frac{d^3 p}{(2\pi)^3} \frac{3e^{-2\beta(E+\mu)}}{1 + 3\bar{\Phi} e^{-\beta(E+\mu)} + 3\Phi e^{-2\beta(E+\mu)} + e^{-3\beta(E+\mu)}} = 0. \end{aligned} \quad (15)$$

By solving the gap equations of the NJL/PNJL models numerically, one obtains the constituent quark mass as a function of temperature and chemical potential for different values of the thermal cutoff Λ_T . The corresponding results are shown in Fig. 1 and Fig. 2, for the NJL and PNJL models, respectively. The critical temperature of the chiral phase transition, T_c , can be defined through the condition

$$T_c : \left. \frac{dM}{dT} \right|_{T=T_c} = \max \left| \frac{dM}{dT} \right|, \quad (16)$$

which characterizes the location of the most rapid change in the constituent quark mass.

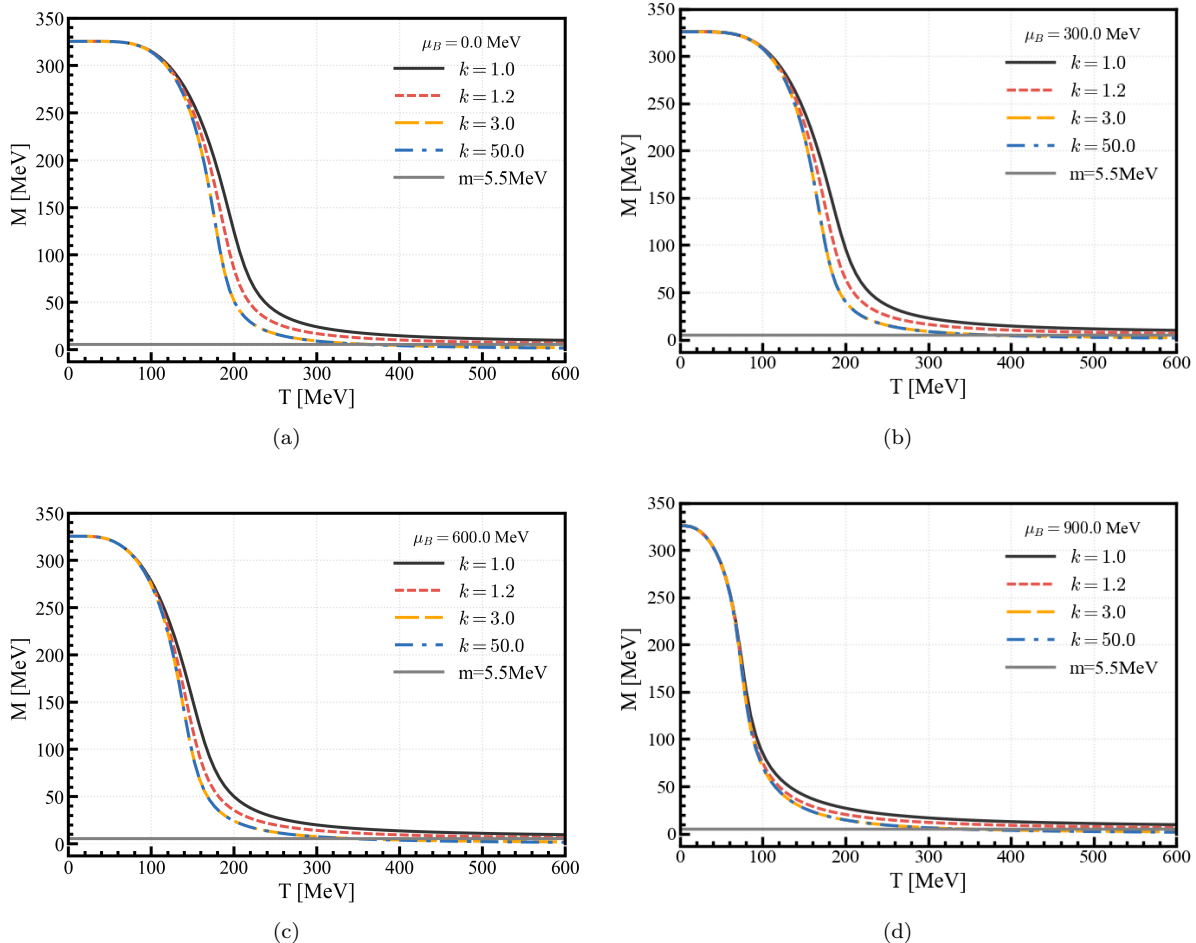


FIG. 1. Constituent quark mass M as a function of temperature T for different truncation factors k (i.e., $\Lambda_T = k\Lambda_0$) at fixed baryon chemical potentials $\mu_B = 0, 300, 600,$ and 900 MeV in the RGNJL model.

As shown in Fig. 1 and Fig. 2, both the NJL and PNJL models exhibit a similar qualitative behavior. In the low-temperature regime, the constituent quark mass remains almost constant and shows only a weak dependence on the choice of Λ_T . This reflects the dominance of the vacuum contribution, where thermal effects are negligible. As the temperature approaches the transition region, however, the dependence on Λ_T becomes pronounced. Larger values of Λ_T lead to an earlier and more rapid decrease of the constituent quark mass, corresponding to a lower pseudo-critical temperature T_c . This behavior indicates that increasing the thermal cutoff effectively enhances the contribution of high-momentum thermal modes, thereby accelerating the restoration of chiral symmetry.

A more detailed inspection of the figures reveals an additional feature. For the case $k = 1.0$, corresponding to $\Lambda_T = \Lambda_0$, the constituent quark mass decreases with increasing temperature but remains above the current quark mass m even at high temperature. In contrast, for larger values of k , the constituent quark mass can drop below the current quark mass in the high-temperature regime. This behavior is unphysical, since the current quark mass sets the lower bound of the dynamical mass in the chirally restored phase.

Beyond the temperature-dependent mass evolution, the structure of the chiral phase boundary—characterized by the critical temperature T_c as a function of the chemical potential of baryon $\mu_B = 3\mu$ —provides further insight into the framework. As illustrated in Fig. 3, both the RGNJL (a) and RGPNJL (b) models exhibit a monotonically decreasing phase boundary as the chemical potential increases. Notably, increasing the parameter k results in a systematic suppression of T_c across the entire range of μ_B . However, this suppression is more pronounced at low chemical potentials; as μ_B approaches 1000 MeV, the curves for varying k tend to converge, suggesting that the sensitivity of the chiral transition temperature to the RG-consistent modification diminishes at high baryon densities.

Therefore, although the RG-consistent extension modifies the thermal contributions and shifts the chiral transition, it does not fully eliminate the artifacts associated with the cutoff prescription. In particular, the appearance of $M < m$

at large k suggests that the RGNJL/RGPNJL framework still requires further refinement to achieve a fully consistent description of the high-temperature regime.

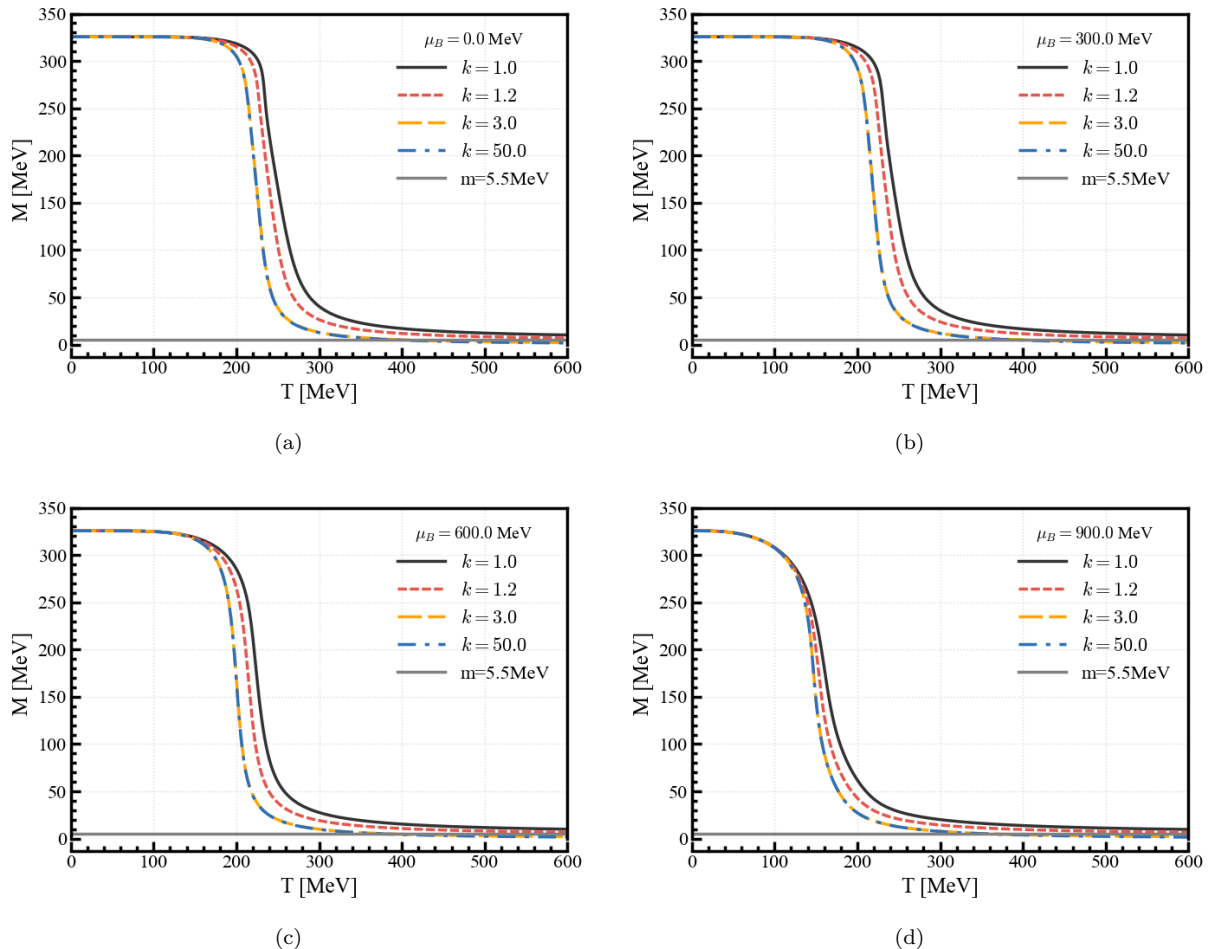


FIG. 2. Constituent quark mass M as a function of temperature T for different truncation factors k (i.e., $\Lambda_T = k\Lambda_0$) at fixed baryon chemical potentials in the RGPNJL model, illustrating the influence of confinement effects.

IV. THERMODYNAMIC QUANTITIES AND BARYON NUMBER FLUCTUATIONS

In addition to the chiral phase transition and the behavior of the constituent quark mass, it is instructive to analyze thermodynamic observables that can be directly derived from the grand potential. These quantities provide complementary information on the equation of state and the response of the system to thermal excitations, and are therefore essential for a comprehensive understanding of the QCD medium [36–38].

The pressure is defined as the negative of the grand potential density, $P = -\Omega$. To ensure a physically meaningful normalization, one subtracts the vacuum contribution such that the pressure vanishes at zero temperature and chemical potential. Accordingly, the pressure is given by

$$P(\mu, T) = \Omega(0, 0) - \Omega(\mu, T), \quad (17)$$

where $\Omega(0, 0)$ denotes the grand potential in vacuum.

The energy density ϵ can be obtained from standard thermodynamic relations,

$$\epsilon = -T^2 \left. \frac{\partial(\Omega/T)}{\partial T} \right|_V = -T \left. \frac{\partial\Omega}{\partial T} \right|_V + \Omega - \Omega(0, 0), \quad (18)$$

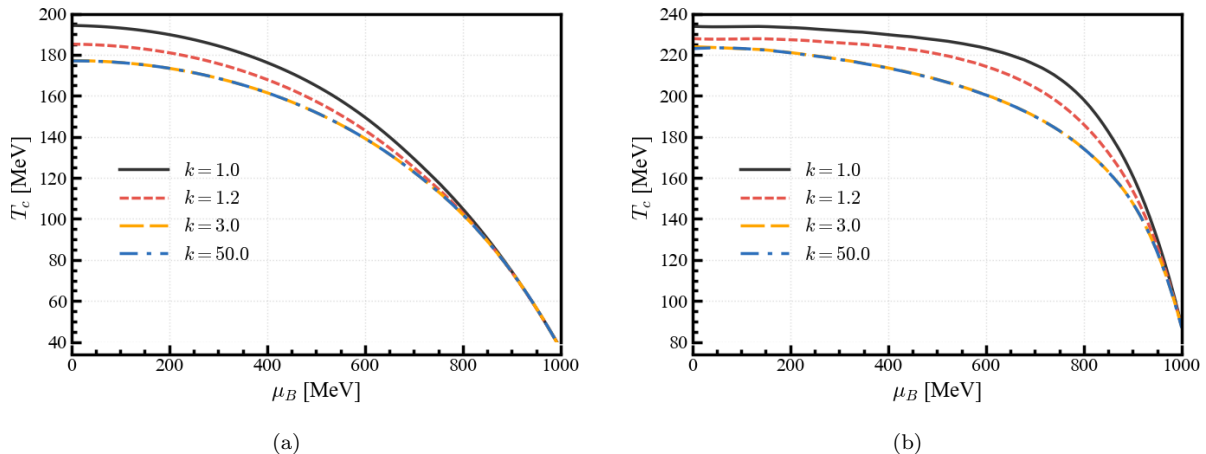


FIG. 3. Chiral phase transition critical temperature T_c versus baryon chemical potential μ_B for the RGNJL (a) and RGPNJL (b) models at different k values.

which explicitly incorporates the vacuum subtraction to maintain consistency with the normalization of the pressure.

The specific heat at constant volume, which characterizes the response of the system to temperature variations, is defined as

$$C_V = \left. \frac{\partial \epsilon}{\partial T} \right|_V = -T \left. \frac{\partial^2 \Omega}{\partial T^2} \right|_V. \quad (19)$$

This quantity is particularly sensitive to the chiral phase transition and typically exhibits a peak structure near the pseudo-critical temperature.

Another important observable is the squared speed of sound, which encodes the stiffness of the equation of state and plays a crucial role in the hydrodynamic evolution of the medium. At constant entropy, it is given by

$$v_s^2 = \left. \frac{\partial P}{\partial \epsilon} \right|_S = \left. \frac{\partial \Omega}{\partial T} \right|_V \bigg/ T \left. \frac{\partial^2 \Omega}{\partial T^2} \right|_V. \quad (20)$$

These thermodynamic quantities serve as independent probes to assess the impact of RG-consistent modifications on the equation of state and to evaluate the validity of the RGNJL and RGPNJL frameworks. As illustrated in Fig. 4 and Fig. 5, both models exhibit a systematic increase in the scaled pressure (P/T^4), energy density ($4\epsilon/T^4$), and specific heat (C_V/T^3) in the high-temperature regime as the parameter k increases, eventually approaching a stable plateau. This behavior aligns with theoretical expectations: at high temperatures, the coupling becomes weak, and the thermal quantities converge toward the Stefan-Boltzmann limit of an ideal, free Fermi gas.

However, a comparison between the two models reveals distinct differences in the transition dynamics. In the RGNJL model (Fig. 4a-c), the thermodynamic quantities exhibit relatively smooth, gradual growth as T/T_c increases. Conversely, the RGPNJL model (Fig. 5a-c) displays significantly steeper growth rates, particularly in the range $0.8 \leq T/T_c \leq 1.2$. The specific heat C_V/T^3 in Fig. 5c exhibits a very sharp, pronounced peak near the pseudo-critical temperature T_c , which is notably more aggressive than the broader, muted peak observed in the RGNJL model (Fig. 4c). This indicates that the inclusion of the Polyakov loop potential in the RGPNJL framework more effectively simulates the rapid change in degrees of freedom associated with the confinement-deconfinement transition.

The behavior of the squared speed of sound (v_s^2) presents a more complex scenario with distinct implications for causality and conformality. In the RGNJL model (Fig. 4d), the baseline ($k = 1.0$) shows an unphysical violation of causality where $v_s^2 > 1$ at high temperatures. However, enforcing the RG consistency condition ($k \rightarrow \infty$) successfully binds v_s^2 to the conformal limit of $1/3$, resolving the violation.

The RGPNJL model (Fig. 5d) demonstrates a more intricate, non-monotonic dependence on k . While both small ($k \approx 1$) and very large ($k \rightarrow \infty$) values of k appear to respect the conformal limit, intermediate values—most notably $k \approx 3.0$ —show the speed of sound rising above the conformal limit ($v_s^2 > 1/3$) for temperatures $T/T_c > 1.5$. This suggests that the RGPNJL framework introduces a non-trivial competition between the chiral sector and the Polyakov loop dynamics. This parametric sensitivity indicates that simply increasing k does not uniformly suppress the speed of sound towards the conformal limit in the presence of Polyakov loops, pointing to a specific parametric region that

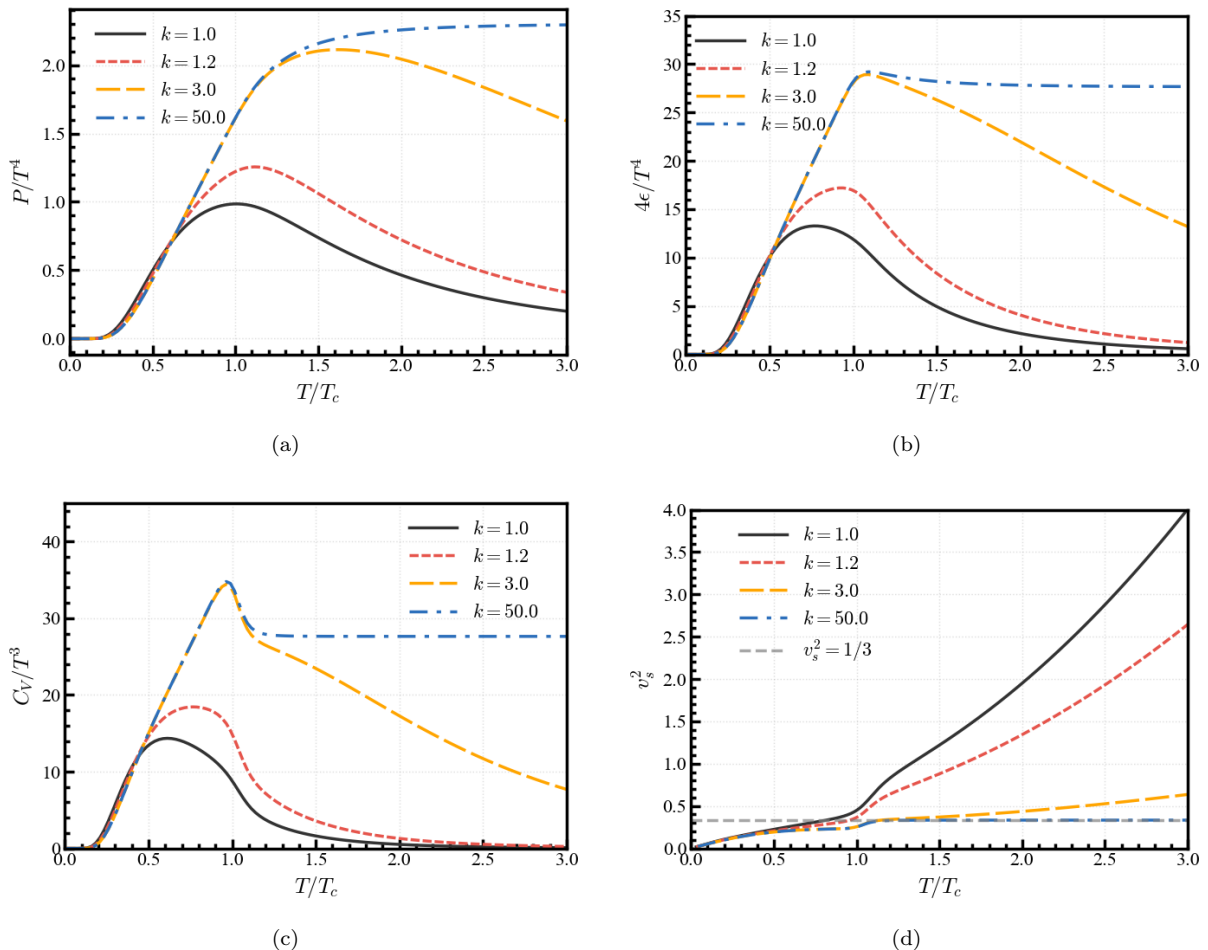


FIG. 4. Thermodynamic quantities as a function of temperature at zero chemical potential for the RGNJL model.

warrants further investigation to reconcile the RG-consistent requirements with the underlying thermodynamics of the model.

The RGNJL model (Fig. 5d) demonstrates a more intricate, non-monotonic dependence on k . While both small ($k \approx 1$) and very large ($k \rightarrow \infty$) values of k appear to respect the conformal limit, intermediate values—most notably $k \approx 3.0$ —show the speed of sound rising above the conformal limit ($v_s^2 > 1/3$) for temperatures $T/T_c > 1.5$. This suggests that the RGNJL framework introduces a non-trivial competition between the chiral sector and the Polyakov loop dynamics. This parametric sensitivity indicates that simply increasing k does not uniformly suppress the speed of sound towards the conformal limit in the presence of Polyakov loops, pointing to a specific parametric region that warrants further investigation to reconcile the RG-consistent requirements with the underlying thermodynamics of the model.

Complementary to the above thermodynamic analysis, the nature of the chiral phase transition can be further elucidated by examining higher-order fluctuations of the net-baryon number. These fluctuations are defined through generalized susceptibilities, χ_n^B , which are derived from the thermodynamic potential Ω (where $P = -\Omega$):

$$\chi_n^B = \frac{\partial^n [P/T^4]}{\partial [\mu_B/T]^n}. \quad (21)$$

The corresponding cumulants of the baryon number distributions, C_n^B , are then expressed as:

$$C_n^B = VT^3 \chi_n^B. \quad (22)$$

By defining the variance $\sigma^2 = C_2^B$ and the kurtosis $\kappa = C_4^B/(\sigma^2)^2$, one can construct the ratio $\kappa\sigma^2$, which serves as a

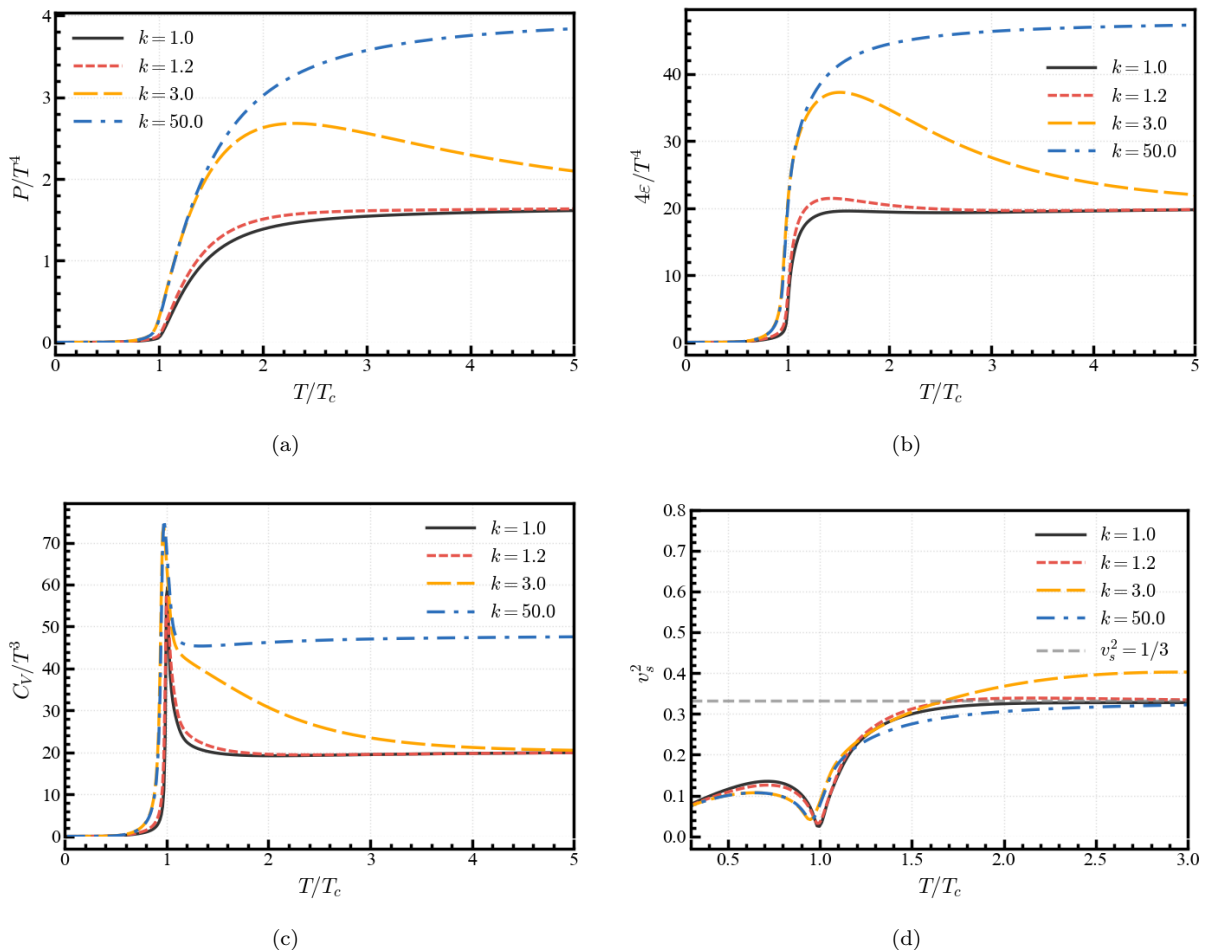


FIG. 5. Thermodynamic quantities as a function of temperature at zero chemical potential for the RGPNJL model.

vital bridge between theoretical framework predictions and experimental observables:

$$\kappa\sigma^2 = \frac{C_4^B}{C_2^B} = \frac{\chi_4^B}{\chi_2^B}. \quad (23)$$

This ratio, $\kappa\sigma^2$, is a highly sensitive indicator of the criticality of the QCD phase transition [40–42]. Utilizing these ratios allows for a rigorous quantitative comparison between the RGNJL/RGPNJL frameworks and lattice QCD data, providing an essential benchmark to determine whether the RG-consistent modifications accurately capture the fluctuation properties of the hot, dense medium.

As illustrated in Fig. 6 and Fig. 7, the behavior of the net-baryon number kurtosis $\kappa\sigma^2$ exhibits distinct characteristics depending on the model and the chemical potential. At vanishing chemical potential ($\mu_B = 0$), the kurtosis in both models remains relatively stable in the low-temperature regime, consistent with the Hadron Resonance Gas (HRG) limit where $\kappa\sigma^2 \approx 1$. As temperature increases, the RGNJL model (Fig. 6a) shows minimal sensitivity to the RG parameter k and significantly underestimates the lattice simulation data in the transition region. In contrast, the RGPNJL model (Fig. 7a) provides a much better qualitative match to the lattice results. In particular, as the RG consistency condition is approached ($k \rightarrow \infty$), the kurtosis in the RGPNJL model exhibits a more rapid decrease for $T/T_c \geq 1.1$, aligning closely with the lattice trend as it approaches the ideal free quark gas (FQG) limit of approximately 0.068.

However, as the chemical potential μ_B increases, the kurtosis develops a severe and non-monotonic dependence on both temperature and the parameter k . In the range $0.8 \leq T/T_c \leq 1.2$, the fluctuations become increasingly volatile: a larger k value leads to a higher maximum and a deeper minimum in the kurtosis. Interestingly, increasing μ_B causes the peak position of the kurtosis to shift toward lower temperatures, a feature observable in both models but significantly magnified in the RGPNJL framework (Fig. 7c and 7d). While the RGNJL model (Fig. 6) maintains

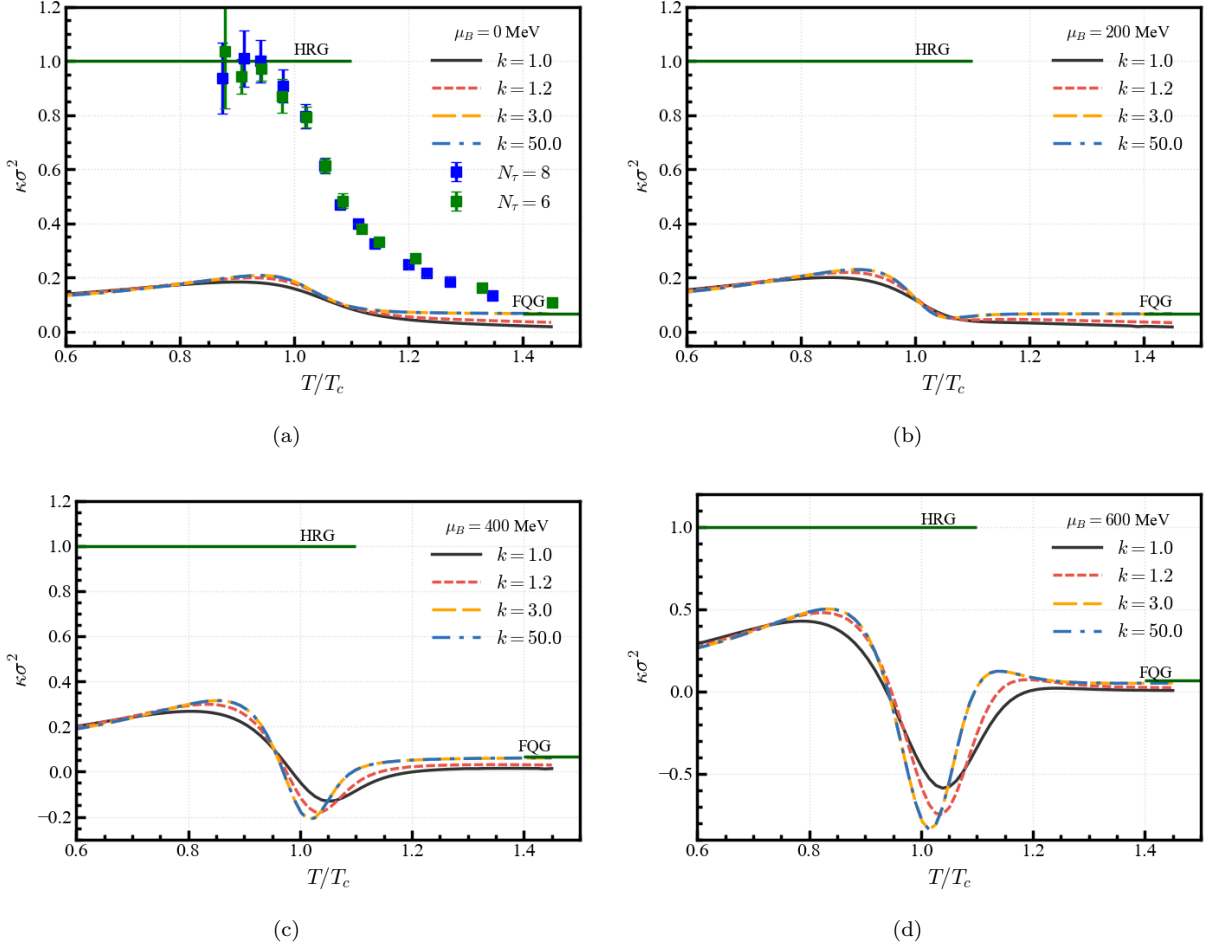


FIG. 6. Net-baryon number kurtosis $\kappa\sigma^2$ as a function of temperature T/T_c for various truncation factors k (where $\Lambda_T = k\Lambda_0$) at fixed baryon chemical potentials $\mu_B = 0, 200, 400,$ and 600 MeV in the RGNJL model. The results for $\mu_B = 0$ are compared with lattice QCD data from [39]. The horizontal lines represent the hadron resonance gas (HRG) limit ($\kappa\sigma^2 = 1$) and the ideal free quark gas (FQG) limit ($\kappa\sigma^2 = 0.068$).

relatively smooth oscillations even at high μ_B , the RGNJL model displays increasingly sharp, "spike-like" structures. For $\mu_B = 600$ MeV, the RGNJL model with $k = 50.0$ displays a sharp oscillation from a positive peak near $\kappa\sigma^2 \approx 4$ to a negative dip below -6 . This dramatic intensification of the extrema near $T/T_c \approx 1.0$ suggests that the coupling between the Polyakov loop and the RG-consistent chiral dynamics heightens the model's sensitivity to the critical point's proximity at high baryon density. These shifts indicate that while RG consistency improves high-temperature thermodynamics, it simultaneously amplifies the signatures of critical fluctuations in the dense medium.

V. CONCLUSION AND DISCUSSION

In this study, we have systematically investigated the impacts of renormalization group (RG) consistency on the thermodynamic properties and chiral phase transitions within the RGNJL and RGNJL frameworks. Our results demonstrate that the implementation of a separate thermal cutoff $\Lambda_T = k\Lambda_0$ significantly modifies the behavior of the constituent quark mass, critical temperature T_c , and higher-order baryon number fluctuations. By increasing the truncation factor k , both models successfully converge toward the expected Stefan-Boltzmann limits at high temperatures, addressing a long-standing limitation of fixed-cutoff effective theories. This convergence confirms that the RG-consistency framework provides a robust method for extending the applicability of non-renormalizable models into the high-energy regime.

A comparative analysis between the RGNJL and RGNJL models reveals both distinct advantages and inherent

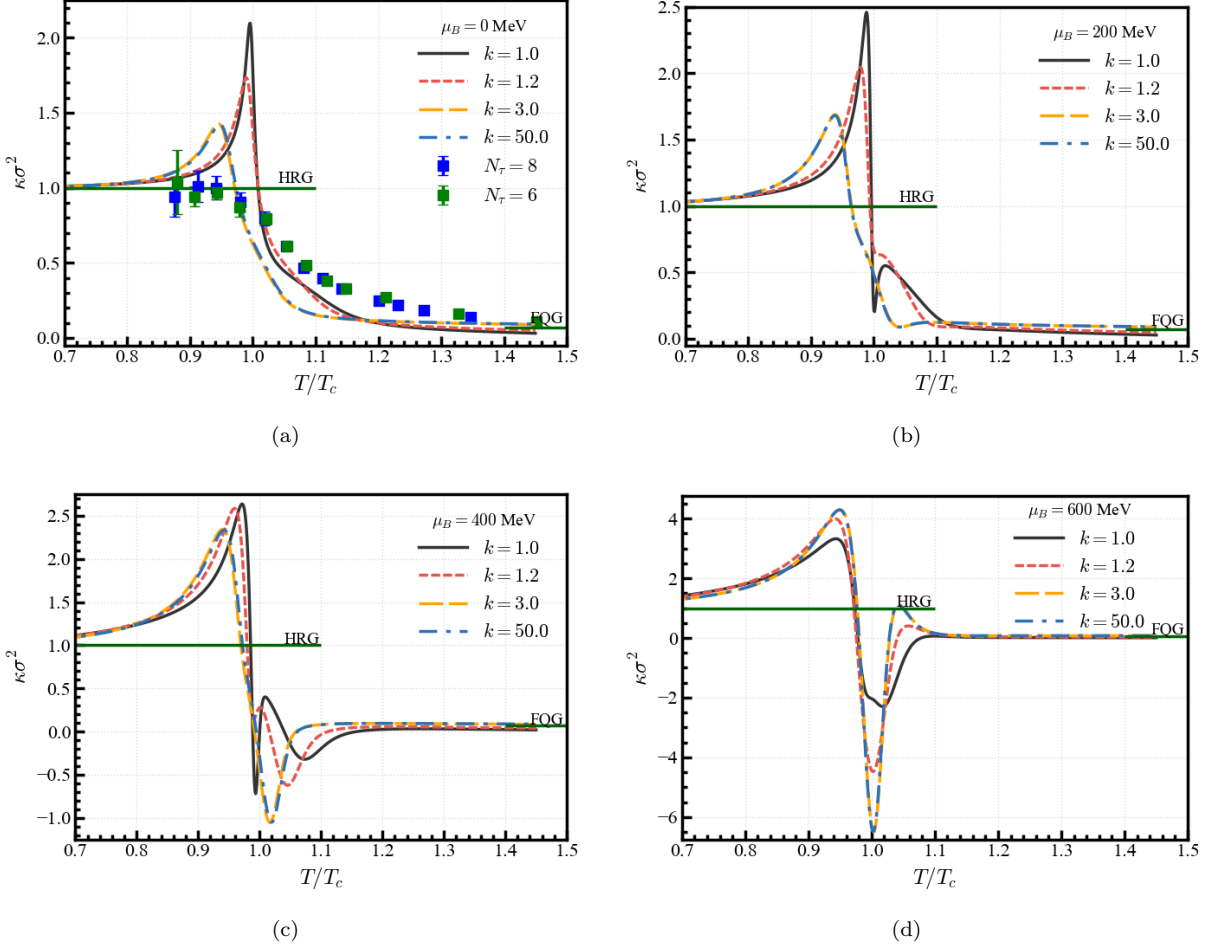


FIG. 7. Net-baryon number kurtosis $\kappa\sigma^2$ as a function of temperature T/T_c for various truncation factors k (where $\Lambda_T = k\Lambda_0$) at fixed baryon chemical potentials $\mu_B = 0, 200, 400,$ and 600 MeV in the RGNJL model. The results for $\mu_B = 0$ are compared with lattice QCD data from [39]. The horizontal lines represent the hadron resonance gas (HRG) limit ($\kappa\sigma^2 = 1$) and the ideal free quark gas (FQG) limit ($\kappa\sigma^2 = 0.068$).

limitations. The primary advantage of the RG-consistent approach is most evident in the RGNJL model's speed of sound, where the enforcement of $k \rightarrow \infty$ effectively resolves the unphysical causality violation ($v_s^2 > 1$) present in the standard NJL baseline. Furthermore, the RGNJL model exhibits superior agreement with lattice QCD data for baryon number kurtosis at vanishing chemical potential, particularly in capturing the sharp transition dynamics near T_c . However, a significant disadvantage persists in both models: for large k , the constituent quark mass can drop below the current quark mass ($M < m$) in the restored phase. This unphysical artifact suggests that while the RG method improves thermal contributions, the current regularization of the vacuum sector and the transition between vacuum and thermal modes require further refinement to maintain the fundamental bounds of the dynamical mass.

Furthermore, the behavior of the squared speed of sound and kurtosis extrema in the RGNJL model points to a non-trivial competition between chiral dynamics and the Polyakov loop potential. We observed that intermediate values of k (e.g., $k \approx 3.0$) can lead to v_s^2 exceeding the conformal limit in the RGNJL framework, a feature not seen in the RGNJL case. This sensitivity suggests that the inclusion of confinement effects through the Polyakov loop introduces additional constraints on the RG parameter space. In the dense medium ($\mu_B > 400$ MeV), the RG-consistent modifications amplify the magnitude of kurtosis oscillations, particularly in the RGNJL model. While this intensification provides a more sensitive probe for searching for the QCD critical point, it also highlights the model's high dependency on the specific parametric choice of the truncation factor in regimes where non-perturbative effects are dominant.

In conclusion, the RG method serves as an essential improvement for NJL-type models by ensuring that high-momentum thermal modes are adequately accounted for, thereby aligning effective theory predictions with the funda-

mental requirements of QCD thermodynamics. The RGPNJL model, in particular, stands out as a more reliable tool for phenomenological comparisons with experimental fluctuation data from the STAR collaboration, provided that k is chosen to satisfy the conformal limit. Future work should focus on developing a more sophisticated interpolation between the vacuum and thermal regulators to eliminate unphysical mass artifacts and on extending this RG-consistent framework to the $(2+1)$ -flavor case to incorporate the effects of strangeness on the QCD phase diagram.

ACKNOWLEDGMENTS

F.L. acknowledges support from the National Natural Science Foundation of China (Grant No. 12547138) and the Anhui University of Science and Technology (Grant No. 2025yjrc0143). X.W. was supported by the Anhui University of Science and Technology under Grant No. YJ20240001.

-
- [1] Kenji Fukushima and Tetsuo Hatsuda. The phase diagram of dense QCD. *Rept. Prog. Phys.*, 74:014001, 2011.
 - [2] Larry McLerran and Robert D. Pisarski. Phases of cold, dense quarks at large $N(c)$. *Nucl. Phys. A*, 796:83–100, 2007.
 - [3] A. Bazavov et al. The chiral and deconfinement aspects of the QCD transition. *Phys. Rev. D*, 85:054503, 2012.
 - [4] Misha A. Stephanov, K. Rajagopal, and Edward V. Shuryak. Signatures of the tricritical point in QCD. *Phys. Rev. Lett.*, 81:4816–4819, 1998.
 - [5] Z. Fodor and S. D. Katz. Critical point of QCD at finite T and mu, lattice results for physical quark masses. *JHEP*, 04:050, 2004.
 - [6] Misha A. Stephanov, K. Rajagopal, and Edward V. Shuryak. Event-by-event fluctuations in heavy ion collisions and the QCD critical point. *Phys. Rev. D*, 60:114028, 1999.
 - [7] B. Friman, F. Karsch, K. Redlich, and V. Skokov. Fluctuations as probe of the QCD phase transition and freeze-out in heavy ion collisions at LHC and RHIC. *Eur. Phys. J. C*, 71:1694, 2011.
 - [8] L. Adamczyk et al. Energy Dependence of Moments of Net-proton Multiplicity Distributions at RHIC. *Phys. Rev. Lett.*, 112:032302, 2014.
 - [9] M. M. Aggarwal et al. An Experimental Exploration of the QCD Phase Diagram: The Search for the Critical Point and the Onset of De-confinement. 7 2010.
 - [10] J. Adam et al. Nonmonotonic Energy Dependence of Net-Proton Number Fluctuations. *Phys. Rev. Lett.*, 126(9):092301, 2021. [Erratum: *Phys.Rev.Lett.* 134, 139902 (2025)].
 - [11] B. E. Aboona et al. Precision Measurement of Net-Proton-Number Fluctuations in Au+Au Collisions at RHIC. *Phys. Rev. Lett.*, 135(14):142301, 2025.
 - [12] Yoichiro Nambu and G. Jona-Lasinio. Dynamical Model of Elementary Particles Based on an Analogy with Superconductivity. I. *Phys. Rev.*, 122:345–358, 1961.
 - [13] Yoichiro Nambu and G. Jona-Lasinio. Dynamical model of elementary particles based on an analogy with superconductivity. II. *Phys. Rev.*, 124:246–254, 1961.
 - [14] S. P. Klevansky. The Nambu-Jona-Lasinio model of quantum chromodynamics. *Rev. Mod. Phys.*, 64:649–708, 1992.
 - [15] Michael Buballa. NJL model analysis of quark matter at large density. *Phys. Rept.*, 407:205–376, 2005.
 - [16] Shijun Mao. Reduction of pseudocritical temperatures of chiral restoration and deconfinement phase transitions in a magnetized PNJL model. *Phys. Rev. D*, 110(5):054002, 2024.
 - [17] Jie Mei, Rui Wen, Shijun Mao, Mei Huang, and Kun Xu. Magnetic catalysis and diamagnetism from pion fluctuations. *Phys. Rev. D*, 110(3):034024, 2024.
 - [18] Mei Huang and Pengfei Zhuang. QCD Matter and Phase Transitions under Extreme Conditions. *Symmetry*, 15(2):541, 2023.
 - [19] Kenji Fukushima. Chiral effective model with the Polyakov loop. *Phys. Lett. B*, 591:277–284, 2004.
 - [20] Kenji Fukushima. Phase diagrams in the three-flavor Nambu-Jona-Lasinio model with the Polyakov loop. *Phys. Rev. D*, 77:114028, 2008. [Erratum: *Phys.Rev.D* 78, 039902 (2008)].
 - [21] Claudia Ratti, Michael A. Thaler, and Wolfram Weise. Phase diagram and thermodynamics of the PNJL model. 4 2006.
 - [22] Lang Yu, Hao Liu, and Mei Huang. Effect of the chiral chemical potential on the chiral phase transition in the NJL model with different regularization schemes. *Phys. Rev. D*, 94(1):014026, 2016.
 - [23] Kai Xue, Xiaozhu Yu, and Xinyang Wang. Do we need to use regularization for the thermal part in the NJL model? *. *Chin. Phys. C*, 46(5):013103, 2022.
 - [24] Sidney S. Avancini, Ricardo L. S. Farias, Norberto N. Scoccola, and William R. Tavares. NJL-type models in the presence of intense magnetic fields: the role of the regularization prescription. *Phys. Rev. D*, 99(11):116002, 2019.
 - [25] Sidney S. Avancini, Ricardo L. S. Farias, and William R. Tavares. Neutral meson properties in hot and magnetized quark matter: a new magnetic field independent regularization scheme applied to NJL-type model. *Phys. Rev. D*, 99(5):056009, 2019.
 - [26] Christof Wetterich. Exact evolution equation for the effective potential. *Phys. Lett. B*, 301:90–94, 1993.

- [27] Jens Braun, Marc Leonhardt, and Jan M. Pawłowski. Renormalization group consistency and low-energy effective theories. *SciPost Phys.*, 6(5):056, 2019.
- [28] Hosein Gholami, Marco Hofmann, and Michael Buballa. Renormalization-group consistent treatment of color superconductivity in the NJL model. *Phys. Rev. D*, 111(1):014006, 2025.
- [29] Hosein Gholami, Ishfaq Ahmad Rather, Marco Hofmann, Michael Buballa, and Jürgen Schaffner-Bielich. Astrophysical constraints on color-superconducting phases in compact stars within the RG-consistent NJL model. *Phys. Rev. D*, 111(10):103034, 2025.
- [30] Fan Lin, Kun Xu, and Mei Huang. Magnetism of QCD matter and the pion mass from tensor-type spin polarization and the anomalous magnetic moment of quarks. *Phys. Rev. D*, 106(1):016005, 2022.
- [31] Nathan Weiss. The Effective Potential for the Order Parameter of Gauge Theories at Finite Temperature. *Phys. Rev. D*, 24:475, 1981.
- [32] Nathan Weiss. The Wilson Line in Finite Temperature Gauge Theories. *Phys. Rev. D*, 25:2667, 1982.
- [33] Kenji Fukushima and Koichi Ohta. Stability of the perturbative vacuum against spatial variations of the Polyakov loop. *J. Phys. G*, 26:1397–1415, 2000.
- [34] C. Ratti, Simon Roessner, M. A. Thaler, and W. Weise. Thermodynamics of the PNJL model. *Eur. Phys. J. C*, 49:213–217, 2007.
- [35] Guo-yun Shao, Zhan-duo Tang, Xue-yan Gao, and Wei-bo He. Baryon number fluctuations and the phase structure in the PNJL model. *Eur. Phys. J. C*, 78(2):138, 2018.
- [36] Claudia Ratti and Wolfram Weise. Thermodynamics of two-colour QCD and the Nambu Jona-Lasinio model. *Phys. Rev. D*, 70:054013, 2004.
- [37] Jin-Li Zhang, Cheng-Ming Li, and Hong-Shi Zong. Discussion of thermodynamic features within the PNJL model. *Chin. Phys. C*, 42(12):123105, 2018.
- [38] Sanjay K. Ghosh, Tamal K. Mukherjee, Munshi G. Mustafa, and Rajarshi Ray. Susceptibilities and speed of sound from PNJL model. *Phys. Rev. D*, 73:114007, 2006.
- [39] A. Bazavov et al. The QCD Equation of State to $\mathcal{O}(\mu_B^6)$ from Lattice QCD. *Phys. Rev. D*, 95(5):054504, 2017.
- [40] Wei-jie Fu, Xiaofeng Luo, Jan M. Pawłowski, Fabian Rennecke, Rui Wen, and Shi Yin. Hyper-order baryon number fluctuations at finite temperature and density. *Phys. Rev. D*, 104(9):094047, 2021.
- [41] Wei-jie Fu, Xiaofeng Luo, Jan M. Pawłowski, Fabian Rennecke, Rui Wen, and Shi Yin. High-order baryon number fluctuations within the fRG approach. *PoS*, CPOD2021:009, 2022.
- [42] Yi Lu, Fei Gao, Xiaofeng Luo, Lei Chang, and Yuxin Liu. Revealing the signal of QCD phase transition in heavy-ion collisions. *Sci. China Phys. Mech. Astron.*, 68(5):251012, 2025.